AKR1C1 Protects Corneal Epithelial Cells Against Oxidative Stress-Mediated Ferroptosis in Dry Eye

Xin Zuo, Hao Zeng, Bowen Wang, Xue Yang, Dalian He, Li Wang, Hong Ouyang, and Jin Yuan

State Key Laboratory of Ophthalmology, Zhongshan Ophthalmic Center, Sun Yat-sen University, Guangdong Provincial Key Laboratory of Ophthalmology and Visual Science, Guangzhou, China

Correspondence: Jin Yuan, State Key Laboratory of Ophthalmology, Zhongshan Ophthalmic Center, Sun Yat-sen University, Guangdong Provincial Key Laboratory of Ophthalmology and Visual Science, Guangzhou 510060, China; yuanjincornea@126.com.

XZ and HZ contributed equally to this work.

Received: December 2, 2021
Accepted: August 2, 2022
Published: September 6, 2022

Citation: Zuo X, Zeng H, Wang B, et al. AKR1C1 protects corneal epithelial cells against oxidative stress-mediated ferroptosis in dry eye. *Invest Ophthalmol Vis Sci.* 2022;63(10):3. https://doi.org/10.1167/iovs.63.10.3

Purpose. To evaluate the precise mode of cell death and to investigate the molecular mechanism underlying the initiation of inflammation in dry eye disease (DED).

Methods. C57BL/6 mice were injected with scopolamine subcutaneously and exposed to desiccating stress to establish a DED mouse model. An immortalized human corneal epithelial cell line (HCEC) was cultured under hyperosmolarity (500 mOsM). Protein expressions were measured using western blot assay and immunofluorescence staining. mRNA expression was analyzed by RNA-sequencing and quantitative RT-PCR. Transmission electron microscopy was used to observe the intracellular ultrastructure. Intracellular Fe^{2+} was detected by a FerroOrange fluorescent probe. Flow cytometry was used to evaluate the cellular reactive oxygen species and lipid peroxidation.

Results. Marked changes in ferroptosis-related markers expression, intracellular iron accumulation, and lipid peroxidation were observed in corneal epithelial cells of DED models. When excessive oxidative stress was suppressed, ferroptosis induced by hyperosmolarity in HCECs was restrained, as indicated by decreased iron content and lipid peroxidation levels. Moreover, AKR1C1 was upregulated by the activation of NRF2 in HCECs under hyperosmolarity. When AKR1C1 was knocked down, cell viability was decreased, accompanied by increased lipid peroxidation, whereas overexpression of AKR1C1 produced the opposite results. It was observed consistently that corneal defects and the inflammatory response were promoted after inhibition of AKR1C1 in vivo.

Conclusions. Excessive oxidative stress-induced ferroptosis participates in DED pathogenesis. The expression of AKR1C1 is triggered by NRF2 to decrease ferroptosis-induced cell damage and inflammation in HCECs. These findings may provide potential makers targeting ferroptosis and AKR1C1 for DED therapy.

Keywords: dry eye disease, ferroptosis, oxidative stress, aldo-keto reductase family 1 member C1, nuclear factor erythroid 2-related factor 2

Dry eye disease (DED) is a common ocular surface disease that affects approximately 5% to 35% of the population worldwide.[1] Chronic activation of inflammation has been considered the key pathogenesis of DED. Dysregulated cell death is the main trigger of initiation and amplification of inflammation.[2,3] In the development of DED, the normal structure and function of corneal epithelial cells are disrupted under the stresses of tear film instability and increased tear osmolality. The disruption, thus, induces the release of a series of innate inflammatory factors, which in turn promotes the development of DED.[1,4] Cell death in DED has been reported to involve necrosis, apoptosis, and pyroptosis.[5] However, the inhibition of these forms of cell death does not completely reverse the damage to corneal epithelial cells in DED, indicating that other modes of cell death are active. Therefore, a more complete picture of the mechanisms of cell death in DED is needed, and the molecular mechanism underlying the initiation of inflammatory injuries in corneal epithelial tissue requires further exploration.

Inflammatory cytokines and various environmental factors, including pollutants, UV radiation and microbial infection, can lead to an increased level of oxidative stress in corneal epithelial cells.[6,7] When excessive reactive oxygen species (ROS) are present, they readily react with proteins, lipids, and nucleic acids, inducing irreversible functional alterations or even complete destruction.[8–10] Our previous research also suggested that the release of abundant ROS would significantly decrease cell viability, thereby promoting inflammation through a positive feedback loop in DED.[11,12] However, the specific mode of cell death and the downstream inflammatory pathways activated under oxidative conditions are not fully defined.

Ferroptosis, an iron-dependent programmed cell death, has been newly identified.[13] Several studies have shown that ferroptosis is centrally involved in the occurrence and development of many diseases, such as acute renal failure, liver fibrosis, neurodegenerative disease, and heart ischemia/reperfusion injury.[14,15] Although the exact mechanism of ferroptosis is not yet well-understood, aberrant

accumulation of lipid peroxides has been identified as a critical mediator of ferroptosis.[16] Because excess lipid peroxides can be neutralized by the enzyme glutathione peroxidase 4 (GPX4), the depletion of GPX4 can directly trigger ferroptosis.[17] Lipid peroxides that fail to be metabolized are oxidized by Fe^{2+} via a Fenton-like reaction, resulting in a large amount of lipid ROS, promoting ferroptosis. The increase in intracellular Fe^{2+} is due to an increase in exogenous iron uptake, facilitated by the upregulation of transferrin receptor (TFRC). Another important molecule regulating the intracellular iron levels is the iron-reducing ferritin, which is composed of ferritin light chain (FTL) and ferritin heavy chain 1 (FTH1).[18] Moreover, the main source of substrates of lipid peroxides are polyunsaturated fatty acids, which are activated by long-chain family member 4 (ACSL4), increasing the risk of lipid peroxidation.[19] Hence, ACSL4 has been identified as an important contributor to ferroptosis.[20] Abnormal expression of any regulator described elsewhere in this article is expected to contribute to ferroptosis. However, little relevant research has focused on the regulatory pathways of ferroptosis in DED. The underlying key factors mediating ferroptosis and the relationship between lipid peroxidation and oxidative stress need to be further explored.

Aldo-keto reductases (AKRs) are a superfamily of proteins that catalyze the reduction of carbonyl substrates dependent on NAD(P)(H).[21] AKR1C1, AKR1C2, and AKR1C3 are members of the AKR 1C subfamily (AKR1Cs). These enzymes play detoxifying roles in cells owing to their antioxidant capacity.[22,23] Under oxidative stress, AKR1Cs can convert a genotoxic byproduct of lipid peroxidase, 4-hydroxy-2-nonenal (4-HNE), into nontoxic 1,4-dihydroxy-2-nonene with high catalytic efficiency.[24] Numerous correlations between AKR1Cs and tumors have been established.[25] Activation of AKR1Cs promotes the proliferation of cancer cells and inhibits the execution of cell death programs, thus exacerbating resistance to cancer chemotherapeutic agents.[26] However, the upstream regulator of AKR1Cs and the crosstalk between AKR1Cs and ferroptosis have not been clarified fully.

In this study, we discovered that excessive oxidative stress-induced ferroptosis participates in the pathogenesis of DED. During this process, AKR1C1 is upregulated to protect corneal epithelial cells from lipid peroxidative damage, triggered mainly by the activation and upregulation of nuclear factor erythroid 2-related factor 2 (NRF2). Furthermore, we confirmed that the inhibition of AKR1C1 promotes the development of ferroptosis in corneal epithelial cells, causing subsequent inflammatory responses and dry eye.

Methods

Reagents and Antibodies

Dulbecco's modified Eagle's medium/F12 medium, penicillin/streptomycin, fetal bovine serum, 0.25% trypsin-EDTA, recombinant human epidermal growth factor, and an insulin-transferrin-selenium supplement were purchased from Invitrogen/Gibco (Carlsbad, CA, USA). Cell culture flasks and 6-, 12-, 24-, and 96-well culture plates were obtained from Corning (Corning, NY, USA). A Cell Counting Kit-8 (CCK-8, #CK04) and FerroOrange fluorescent probe (#F374) were purchased from Dojindo Laboratories (Kumamoto, Japan). C11-BODIPY581/591 (#D3861) was purchased from Invitrogen. Anti-AKR1C2 (#13035), anti-NRF2 (#12721), anti-TFRC (#13113), anti-glyceraldehyde-3-phosphate dehydrogenase (#5174), horseradish peroxidase–conjugated anti-rabbit IgG (#7076), horseradish peroxidase–conjugated anti-mouse IgG (#7072), Alexa Fluor 488–labeled donkey anti–rabbit IgG (#4412), Alexa Fluor 488-labeled donkey anti-mouse IgG (#4409) antibodies, and DAPI (#4083) were purchased from Cell Signaling Technology (Danvers, MA, USA). The following antibodies were purchased from Abcam (Cambridge, UK): anti-AKR1C1 (#192785), anti-AKR1C3 (#209899), anti-HO1 (#68477), anti-GPX4 (#125066), anti-FTH (#65080), anti-FTL (#69090), and anti-ACSL4 (#155282). MPA (#HY-B0648) was purchased from MedChemExpress (Monmouth Junction, NJ, USA). Fer-1 (#SML0583), NAC (#A9165), *tert*-butyl hydroperoxide (#458139), BRU (#SML1868), and other reagent-grade chemicals were purchased from Sigma-Aldrich (St. Louis, MO, USA) unless otherwise indicated.

Cell Culture and Development of the Hyperosmolar Stress Model

The human SV40 immortalized corneal epithelial cell line (CRL-11135, human corneal epithelium [HCE-2]) was purchased from ATCC (Manassas, VA, USA). HCE-2 cells were cultured on plates in a humidified atmosphere containing 5% carbon dioxide (CO_2) at 37°C. Dulbecco's modified Eagle's medium/F12 containing 5 µg/mL insulin, 10 ng/mL human epidermal growth factor, 10% fetal bovine serum, and 1% penicillin/streptomycin was used as the culture medium. HCE-2 cells were then treated for 24 hours in iso- or hyperosmolar (312 or 500 mOsM, respectively) medium. Hyperosmolarity was achieved by adding 94 mM sodium chloride.

Animal Model and Treatment

A total of 72 female C57BL/6J mice aged 6 to 8 weeks were purchased from Beijing Vital River Laboratory Animal Technology Co., Ltd. (Beijing, China). The mice in the dry eye model were housed in an environmentally controlled room maintained at 30% humidity or less and were exposed to a continuous air draft created by fans. The mice were injected subcutaneously with scopolamine hydrobromide (1.5 mg/0.3 mL; Sigma–Aldrich) three times daily for 5 consecutive days. Control mice matched for age and sex were maintained in an environment of 50% to 75% relative humidity. All animal experiments complied with the ARVO Statement for the Use of Animals in Ophthalmic and Vision Research and were approved by the Institutional Review Board of Zhongshan Ophthalmic Center (Guangzhou, China; approval ID: 2020-138). Each mouse in the experimental treatment groups was intraperitoneally injected with 400 µL of a solution of Fer-1 (0.1 mg/mL; in 10% DMSO) or MPA (1 mg/mL; in 10% DMSO). The same volume of 10% DMSO was injected as a control.

Sodium Fluorescein Staining of the Corneal Epithelium

The inferior lateral conjunctival sac was treated with sodium fluorescein to evaluate the degree of corneal epithelial defects in mice. Corneal epithelial images were acquired by two independent technicians using a cobalt blue filter in a slit-lamp microscope imaging system (SL-D7/DC-3/MAGENet; Topcon, Tokyo, Japan). Corneal defects were quantified with ImageJ software (National Institutes of Health Bethesda, MD): corneal defect coverage area

(%) = (fluorescein sodium-positive area/whole corneal area) × 100%.

Cell Viability Assay

A CCK-8 assay was performed according to the manufacturer's protocol to evaluate cell viability. In brief, HCECs were seeded in 96-well plates and exposed to conditioned medium. Then, 100 µL of a mixture of culture medium and CCK-8 solution was added to each well of the plates. The plates were then incubated for 1 to 2 hours (37°C, 5% CO_2). The absorbance at 450 nm was measured by using a microplate reader (BioTek Instruments, Winooski, VT, USA).

Measurement of Intracellular ROS and Lipid Peroxidation

Intracellular ROS levels were measured using a 2′,7′-dichlorofluorescein diacetate (H2DCFDA) assay kit (Abcam, #ab113851). In brief, HCECs were grown in conditioned medium in six-well plates. When confluent, the cells were rinsed and incubated with 10 µM H2DCFDA at 37°C for 30 minutes. Subsequently, the reaction mixture was replaced with 500 µL of PBS. Lipid peroxidation was assessed by treatment with C11-BODIPY581/591 according to the manufacturer's protocol. HCECs were first seeded in six-well plates and exposed to conditioned medium. When confluent, the cells were rinsed and incubated with 5 µM C11-BODIPY working solution at 37°C for 30 minutes. Then, the reaction mixture was replaced with 1 mL of PBS. The levels of intracellular ROS and lipid peroxidation were measured separately by flow cytometry (BD LSRFortessa, San Jose, CA, USA).

Measurement of Intracellular Fe^{2+}

A FerroOrange fluorescent probe was used according to the manufacturer's protocol for the detection of intracellular Fe^{2+}. In brief, HCECs were grown in conditioned medium in 24-well plates. Subsequently, the cells were rinsed and incubated with 250 µM FerroOrange for 30 minutes. After washing with PBS, the cells were observed under an inverted fluorescence microscope (Leica Biosystems, Wetzlar, Germany; DMi8). Fe^{2+} fluorescence intensity was quantified with ImageJ software.

RNA Interference

HCECs were transfected using Lipofectamine RNAiMAX Transfection Reagent (Invitrogen, #13778150) with the following siRNAs: AKR1C1—sense, 5′-GUUUAGAGGCCACC AAAUUTT-3′, antisense, 5′-AAUUUGGUGGCCUCUAAAGTT-3′; AKR1C2—sense, 5′-CUGCACAUGUUU ACAAUAATT-3′, antisense, 5′-UUAUUGUAAACAUGUGCAGTT-3′; AKR1C3—sense, 5′-GAAUGUCAUCCGUAUUUCATT-3′, antisense, 5′-UGAAAUACGGAUGACAUUCTT-3′; and HMOX-1—sense, 5′-GCAGAGAAUGCUGAGUUCAUGAGGA-3′, antisense, 5′-UCCUCAUGAACUCAGCAUUCUCUGC-3′. A nontargeting scramble siRNA was used as a negative control treatment (Invitrogen). In brief, the siRNA was dissolved in nuclease-free water to a final concentration of 10 µM. Subsequently, 5 µL of the siRNA and 9 µL of lipofectamine RNAiMAX were added to 150 µL of Opti-MEM. Then, the solution of siRNA and lipofectamine RNAiMAX was mixed and incubated at room temperature for 5 minutes to allow complex formation. Then, equal volumes of the mixture were added to the culture plates. Twenty-four hours later, the medium was replaced with conditioned medium.

AKR1C1 Overexpression

The AKR1C1 gene was cloned into pCDH-copGFP-T2A-Puro by XbaI-NotI double digestion. The AKR1C1-specific overexpression vector and empty vector were designed and constructed by Tsingke Biotechnology (Beijing, China). The recombinant lentiviral plasmid was transfected into 293T cells to produce recombinant lentivirus. Then, the lentiviral vectors were transfected into HCECs according to the manufacturer's instructions. In brief, HCECs were seeded in six-well plates and cultured to 40% to 60% confluence. Then, the HCECs were transfected with the corresponding lentivirus. After 36 hours of transfection, the cells were subcultured for the following experiments.

Western Blot Analysis

Total cellular and corneal protein was extracted with a Minute Total Protein Extraction Kit (Invent Biotechnologies, #SD001). A bicinchoninic acid protein assay kit (Millipore, Billerica, MA, USA) was used to measure the total protein concentration. Then, equal amounts of protein samples were loaded onto sodium dodecyl sulfate-polyacrylamide gels and electrophoresed. The separated proteins in the gels were transferred to polyvinylidene fluoride membranes (Millipore, Bedford, MA, USA). After blocking the membranes with 5% nonfat milk in Tris-buffered saline with Tween 20 for 2 hours at room temperature, the membranes were incubated with the appropriate primary antibodies overnight. After the membranes were rinsed thoroughly, they were further incubated with secondary antibodies for 1 hour at room temperature. An ECL kit (Vazyme, #E411) was used to magnify the horseradish peroxidase signals, which were detected with a Bio-Rad (Bio-Rad Laboratories, Inc., Berkeley, CA, USA) Western blot detection system. Grayscale images of the Western blots were used for semiquantitative analysis with ImageJ software.

RNA-Sequencing (RNA-Seq) Analysis

RNA extraction from the HCEC and C57BL/6J mouse cornea samples was performed using an RNeasy Mini Kit (Qiagen, Valencia, CA, USA; #74106). A TruSeq Stranded mRNA Library Prep kit (Illumina, San Diego, CA, USA; #20020594) was used to construct the RNA-seq libraries. Total RNA was sequenced on Illumina PE150 sequencers. Sequencing reads were mapped to hg19 using STAR. Transcript per million values were calculated using the relative standard error of the mean. Differential expression was determined using DESeq2. Differentially expressed genes were defined at a P value of less than 0.01 as well as a $\log_2$-fold change of greater than 1. Two or three biological samples in each group were applied to the RNA-seq data.

Quantitative RT-PCR (qRT-PCR)

Total RNA from HCECs or intact corneas was extracted with an RNeasy Mini Kit (Qiagen) according to the manufacturer's instructions. Total RNA was quantified with a spectrophotometer (NanoDrop ND-1000; ThermoFisher Scientific,

Investigative Ophthalmology & Visual Science

Waltham, MA, USA). cDNA was synthesized with PrimeScript RT Master Mix (TAKARA BIO INC, Shiga, Japan) and was then amplified with SYBR Green Supermix (Bio-Rad Laboratories, Inc.) in a Light Cycler 480 Real-Time PCR System with designed primers. Glyceraldehyde-3-phosphate dehydrogenase served as the internal reference gene. The sequences of the primers are shown in Supplementary Table S1.

Immunofluorescence Staining

For cell immunofluorescence staining, HCECs were grown in 24-well plates containing a cover glass in each well. After different treatments, the cells were sequentially washed with PBS, fixed with 4% paraformaldehyde for 10 minutes, blocked with 3% BSA containing 0.3% Triton X-100 for 1 hours, and incubated overnight at 4°C with the primary antibodies. After washing, the cells were incubated for 1.5 hours with the secondary antibody. Images were acquired using an inverted fluorescence microscope (Leica Biosystems, DMi8).

For corneal immunofluorescence staining, mice were euthanized, and their eyeballs were excised. After fixation and paraffin embedding, the eyeballs were sectioned. Slices were dewaxed with dimethylbenzene and then subjected to high pressure for antigen retrieval. The remaining steps were performed as previously described for cell immunofluorescence staining. Fluorescence intensity was quantified with ImageJ software.

TUNEL Staining

A TUNEL FITC Apoptosis Detection Kit (Vazyme Biotechnology, Nanjing, China) was used for the TUNEL assay according to the manufacturer's instructions. In brief, paraffin-embedded corneal sections were dewaxed with dimethylbenzene and blocked with 3% BSA containing 0.3% Triton X-100 for 1 hour. Then, the sections were incubated with TUNEL reaction mix at 37°C for 1 hour. Fluorescence was observed with an inverted fluorescence microscope (Leica Biosystems, DMi8). TUNEL-positive cells were quantified with ImageJ software: TUNEL-positive cells (%) = (fluorescein TUNEL-positive area/whole image area) × 100%.

Transmission Electron Microscopy

HCECs were fixed with 2.5% glutaraldehyde and 150 mM sodium cacodylate (pH 7.4) at 4°C overnight. HCECs were postfixed in 1% osmium (VIII) oxide (OsO_4) followed by uranyl acetate, dehydrated in ethanol and embedded in epoxy resin. A Hitachi (HT7700, Tokyo, Japan) transmission electron microscope system was used to examine the sections.

Statistical Analysis

All data are expressed as the mean ± standard deviation. Statistical analyses were performed using GraphPad Prism (GraphPad, San Diego, CA). The Student *t* test was used to compare differences between groups. One- or two-way ANOVA followed by Bonferroni's post hoc test was used for comparisons among three or more groups. A *P* value of less than 0.05 was considered to indicate statistical significance.

Results

Corneal Epithelial Cells Undergo Ferroptosis in Dry Eye

To explore whether ferroptosis occurs in corneal epithelial cells in dry eye, HCECs were exposed to hyperosmolarity to establish a DED model in vitro for RNA sequencing. Kyoto Encyclopedia of Genes and Genomes (KEGG) pathway enrichment analysis of differentially expressed genes between the Ctr group and the hyperosmolarity group showed that ferroptosis was included in the top 20 enrichment pathways (Fig. 1a and Supplementary Table S2). In the sequencing results, the ferroptosis-related genes were first divided into three categories based on their regulatory functions. Then the genes with obvious changes in each of the three pathways were selected to explore the specific mechanism of ferroptosis in dry eye (Fig. 1b and Supplementary Table S3). Among these genes, we confirmed that the mRNA expression of a negative regulator (GPX4) was decreased and that of positive regulators (TFRC and ACSL4) was increased in HCECs under hyperosmolar conditions (Supplementary Fig. S1). However, unlike its mRNA expression, a decreasing trend was observed for the protein expression of ACSL4 (Supplementary Fig. S1 and Fig. 1c). In addition, the negative regulators FTL and FTH1 were upregulated (Supplementary Fig. S1 and Fig. 1c), and these regulators were reported to combine with iron to decrease the cell damage caused by free iron. To further investigate the intracellular iron content, a FerroOrange fluorescent probe was applied. Compared with the control group, the density of red fluorescence representing the intracellular Fe^{2+} content was increased significantly in HCECs under hyperosmolarity. (Fig. 1d). These data indicated that the upregulated FTL and FTH1 may fail to completely bind the excess intracellular iron. To better distinguish the morphologic changes associated with ferroptosis in hypertonic HCECs, HCECs were treated with (1S,3R)-RSL3 (RSL3), which induces ferroptosis upon inactivating GPX4, as a positive control. Transmission electron microscopy demonstrated considerable shrinkage of mitochondria with increased membrane density and the disappearance of mitochondrial cristae, typical to morphologic characteristics of ferroptosis, in both the hyperosmolarity and RSL3 groups (Fig. 1e). Lipid peroxide generation evaluated by the fluorescence of the specific probe BODIPY C11 showed evident accumulation of lipid peroxides in HCECs subjected to hyperosmolar stress (Fig. 4b). Collectively, our findings confirmed that ferroptosis was induced in HCECs in DED.

The Ferroptosis Inhibitor Ferrostatin-1 (Fer-1) Alleviates Dry Eye In Vivo

RNA sequencing and KEGG pathway enrichment analysis were also performed in vivo to compare and analyze the untreated group and the desiccation stress (DS)-treated group. The results indicated that ferroptosis occurred in the corneal epithelial cells of DS mice (Figs. 2a, b, Supplementary Tables S4 and S5). The important ferroptosis-related markers GPX4, TFRC, FTL, and FTH1 showed the same expression trend as in vitro, as demonstrated by qRT-PCR, immunofluorescence staining, and Western blot (Figs. 2c, d and Supplementary Figs. S2a–c). Interestingly, the expression of ACSL4, which is recognized as an important regulator facilitating the synthesis of polyunsaturated fatty acids

Investigative Ophthalmology & Visual Science

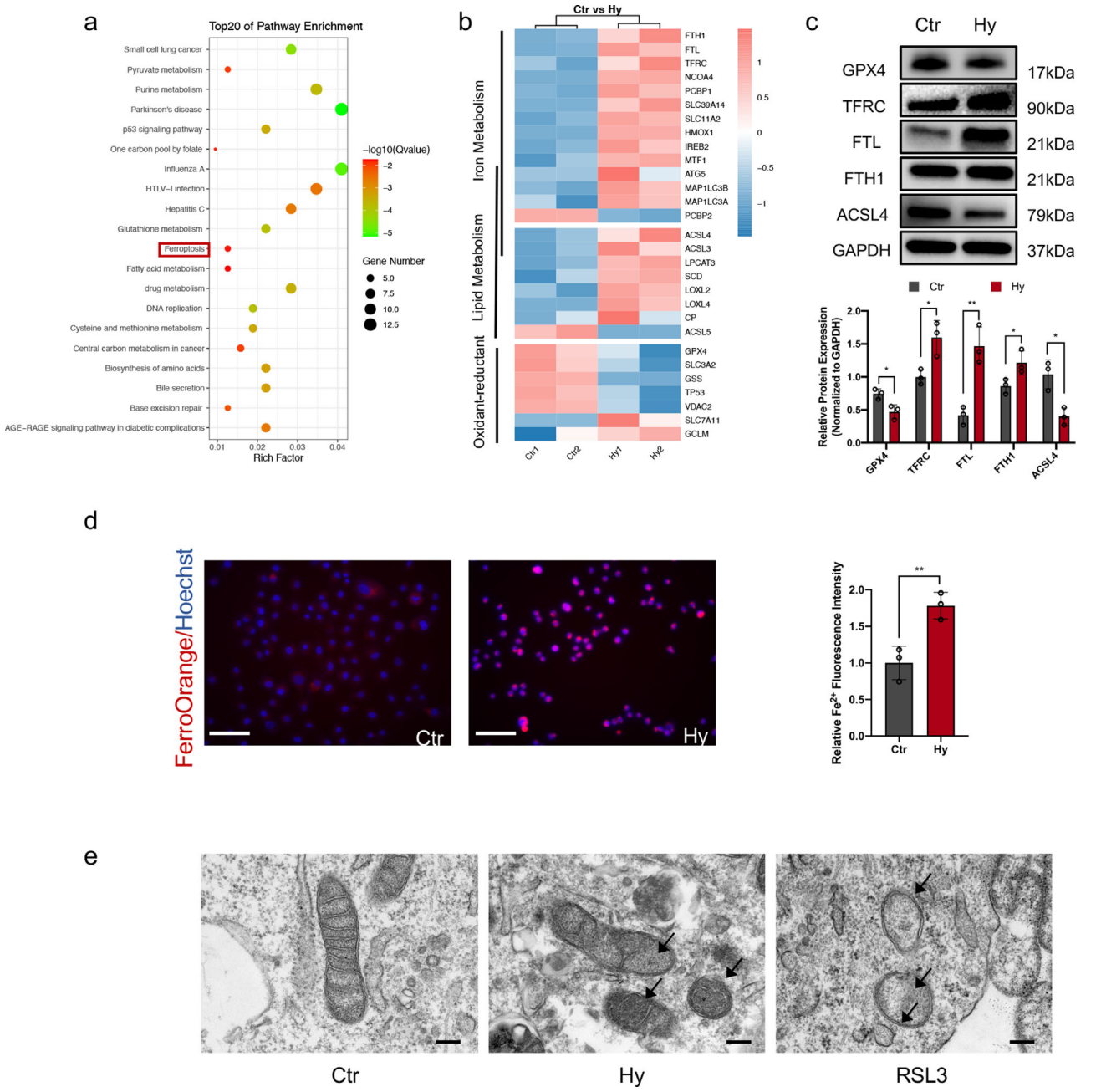

Figure 1. HCECs undergo ferroptosis under hyperosmolarity. (**a**) Top 20 KEGG pathway enrichment analyses in HCECs cultured in hyperosmotic medium (Hy, 500 mOsM) relative to those cultured in normal medium (Ctr) for 24 hours (two samples per group). (**b**) Heatmap showing the transcriptional changes in ferroptosis-related genes in the two groups. (**c**) Representative immunoblots for GPX4, TFRC, FTL, FTH1, and ACSL4 in control and hyperosmolarity-treated HCECs. Glyceraldehyde-3-phosphate dehydrogenase (GAPDH) was used as the loading control. Relative protein expression levels were calculated with ImageJ and normalized to GAPDH. $N = 3$ per group. (**d**) Intracellular Fe^{2+} was detected with the FerroOrange probe under an inverted fluorescence microscope (*blue*, Hoechst-stained nuclei; *red*, FerroOrange-stained Fe^{2+}). Scale bar, 100 µm. The Fe^{2+} fluorescence intensity was quantified by ImageJ. (**e**) HCECs were cultured in normal medium, hyperosmotic medium or normal medium containing (1S,3R)-RSL3 (RSL3, 5 µM). Representative ultrastructural micrographs were acquired by transmission electron microscopy. The hyperosmolarity and RSL3 groups showed shrinkage of mitochondria, increased membrane density, and the disappearance of mitochondrial cristae. Black arrows indicate those typical morphologic characteristics. Scale bar, 2 µm. $^{*}P < 0.05$; $^{**}P < 0.01$.

and induction of ferroptosis, was increased and had the most marked change in the in vivo DED model (Fig. 2c and Supplementary Figs. S2a, b). Next, to further explore the relationship between ferroptosis and ocular surface defects in dry eye, Fer-1 (0.1 mg/mL, 400 µL, in 10% DMSO every day), a specific inhibitor of ferroptosis,[27] was intraperitoneally injected into DED model mice. Because 4-HNE is considered a byproduct of lipid peroxidation,[28] immunofluorescence staining of 4-HNE was used to indicate the level of lipid peroxidation in vivo. Fer-1 availability rescued the ocular surface defects (Figs. 3a, b), decreased the death of corneal epithelial cells (Figs. 3c, d), and significantly

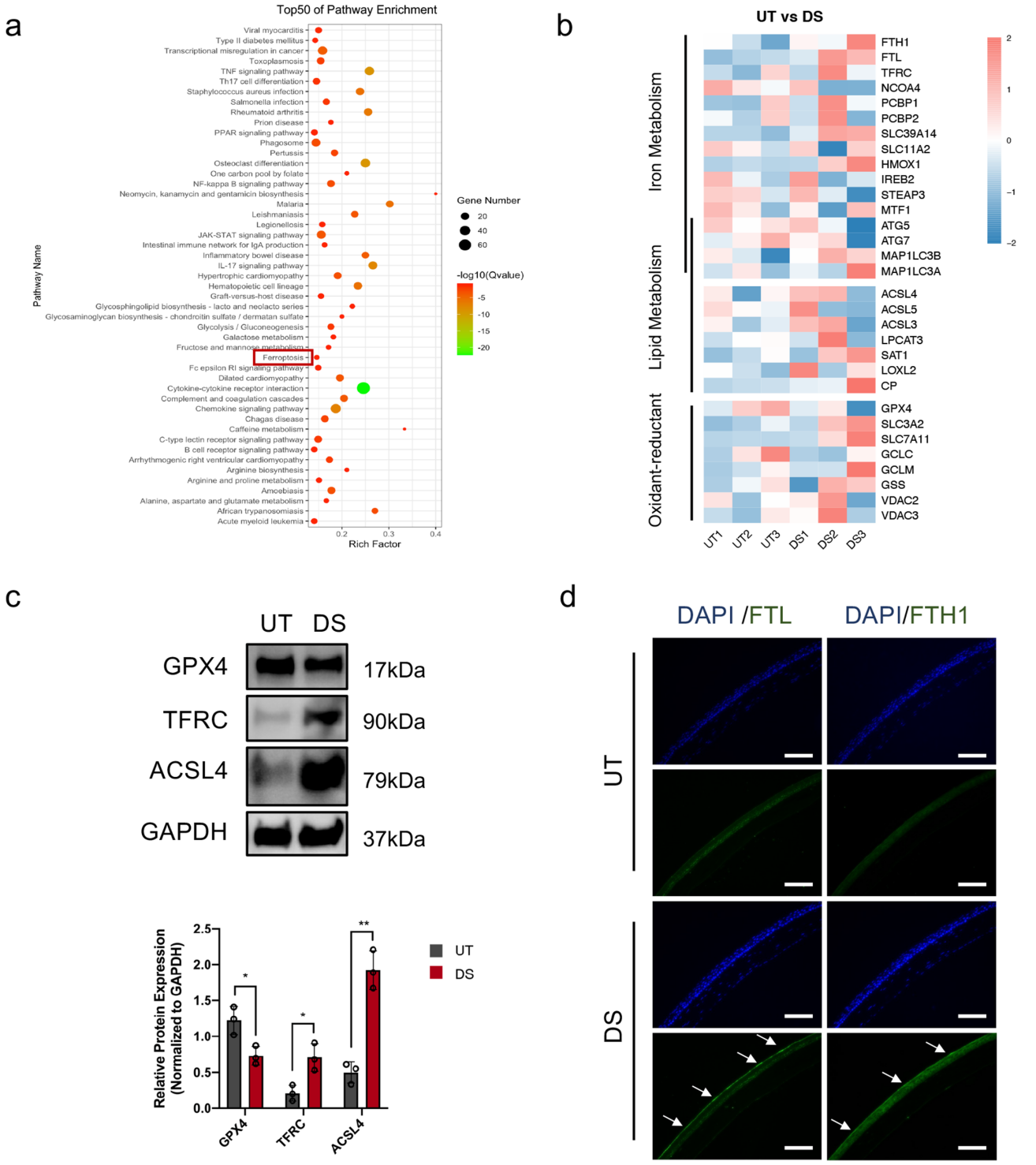

Figure 2. Corneal epithelial cells underwent ferroptosis in a mouse model of DED. Experimental group mice were subjected to DS for 5 days. (**a**) Top 50 KEGG pathway enrichment analysis in corneas from untreated (UT) mice and DS mice. (**b**) Heatmap showing the transcriptional changes in ferroptosis-related genes in the two groups (three samples per group). (**c**) Representative immunoblots for GPX4, TFRC, and ACSL4 of the UT and DS groups. Glyceraldehyde-3-phosphate dehydrogenase (GAPDH) was used as the loading control. Relative protein expression levels were calculated with ImageJ and normalized to GAPDH. $N = 3$ per group. $^{*}P < 0.05$, $^{**}P < 0.01$. (**d**) Representative fluorescence images showing the expression of FTL, FTH1 in the corneal epithelium in the UT and DS groups. *White arrows* indicate the marked positive-expression area of FTL, FTH1 (*blue*, DAPI-stained nuclei; *green*, anti-FTL, anti-FTH1 antibody staining-positive cells) Scale bar, 100 µm.

decreased 4-HNE expression compared with that in the untreated DED model mice (Figs. 3e, f). To evaluate the severity of dry eye and explore the relationship between ferroptosis and inflammation, we evaluated the expression

Investigative Ophthalmology & Visual Science

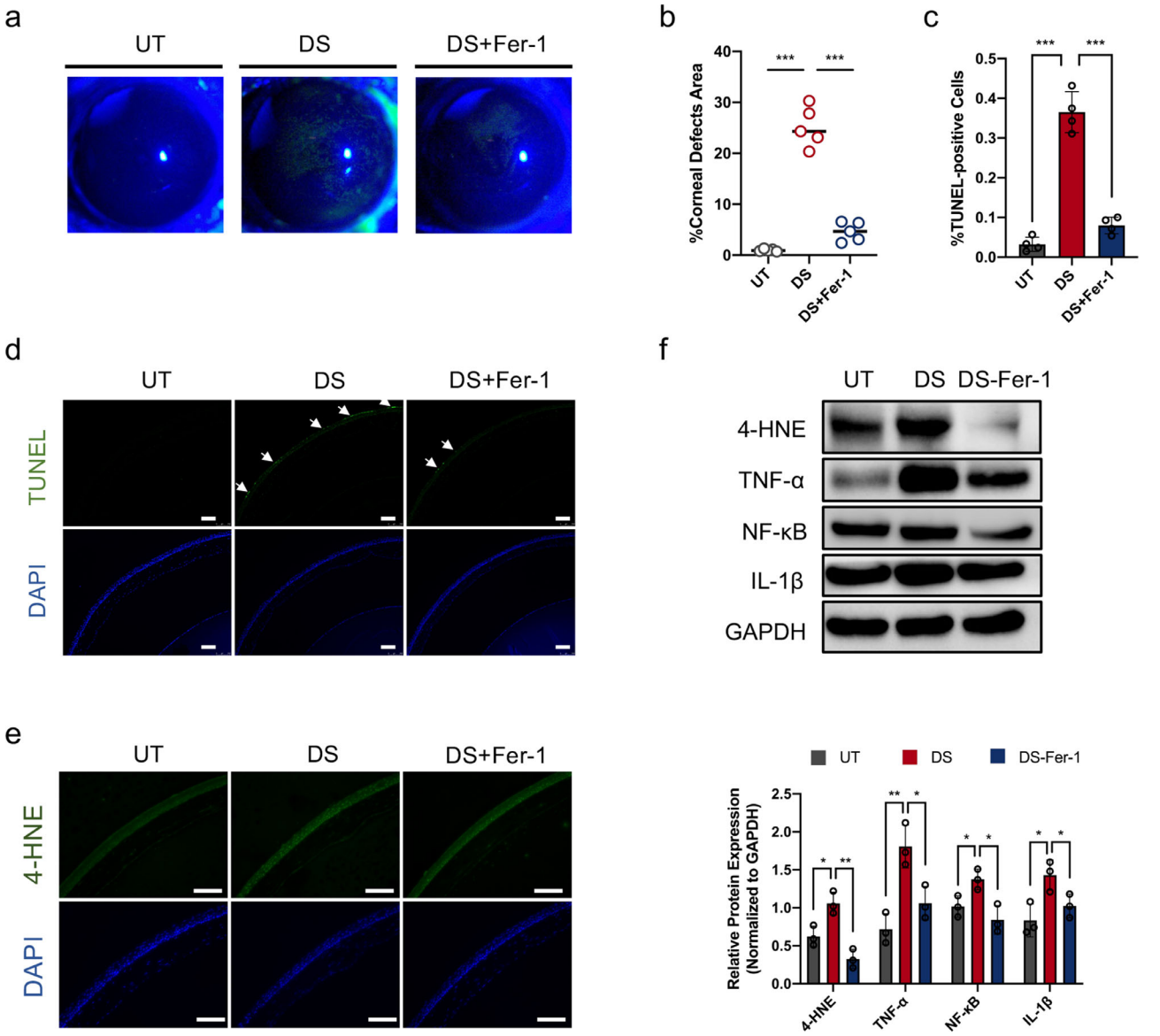

Figure 3. Fer-1 alleviates corneal defects and the inflammatory response in vivo. (**a**) Photographs of corneal fluorescein staining. (**b**) The corneal defect area (percentage) was calculated with ImageJ. $N = 5$ per group. (**c**) The percentage of TUNEL-positive cells was determined with ImageJ. $N = 4$ per group. (**d**) Representative fluorescence images from the TUNEL assay of the corneal epithelium from UT mice, DS mice and DS mice treated with ferrostain-1 (Fer-1) (*blue*, DAPI-stained nuclei; *green*, TUNEL-stained dead cells). *White arrows* indicate TUNEL-positive cells. Scale bar, 100 µm. (**e**) Representative fluorescence images showing the expression of 4-HNE in the corneal epithelium of UT, DS, and DS-Fer-1 mice. Scale bar, 100 µm. (**f**) Representative immunoblots for 4-HNE, TNF-α, NF-κB, and IL-1β of the UT, DS, and DS-Fer-1 groups. Glyceraldehyde-3-phosphate dehydrogenase (GAPDH) was used as the loading control. Relative protein expression levels were calculated with ImageJ and normalized to GAPDH. $N = 3$ per group. $^{*}P < 0.05$, $^{**}P < 0.01$, $^{***}P < 0.001$.

levels of the typical DED-associated inflammatory pathway nuclear factor-κB (NF-κB) and the inflammatory factors tumor necrosis factor-α (TNF-α) and IL-1β. It is found that Fer-1 effectively decreased the protein expression of TNF-α, NF-κB, and IL-1β in DED mice (Fig. 3f). These results suggested that ferroptosis promoted the damage to corneal epithelial cells and the development of inflammation in dry eye, which could be partially reversed by Fer-1.

Oxidative Stress Induces Ferroptosis in Dry Eye

Activation of oxidative stress in corneal epithelial cells in dry eye has been proven in many studies, and our studies also confirmed this conclusion (Fig. 4a). More recently, ferroptosis has been identified to be involved in oxidative stress-induced cell death in numerous diseases. To explore the role of oxidative stress in ferroptosis induction in DED, *N*-acetylcysteine (NAC), an ROS scavenger, was used to treat HCECs with and without hyperosmolar stress. The increases in the generation of lipid peroxides and the iron content with hyperosmolarity were abrogated by NAC (Fig. 4b and Supplementary Fig. S3). Correspondingly, after NAC treatment, the expressions of TFRC, FTL, and FTH1 have decreased, and GPX4 expression was upregulated (Figs. 4c, d). To further demonstrate the relationship between oxidative stress and ferroptosis, HCECs were exposed to 400 µM *tert*-butyl hydroperoxide, a common inducer of oxidative

Investigative Ophthalmology & Visual Science

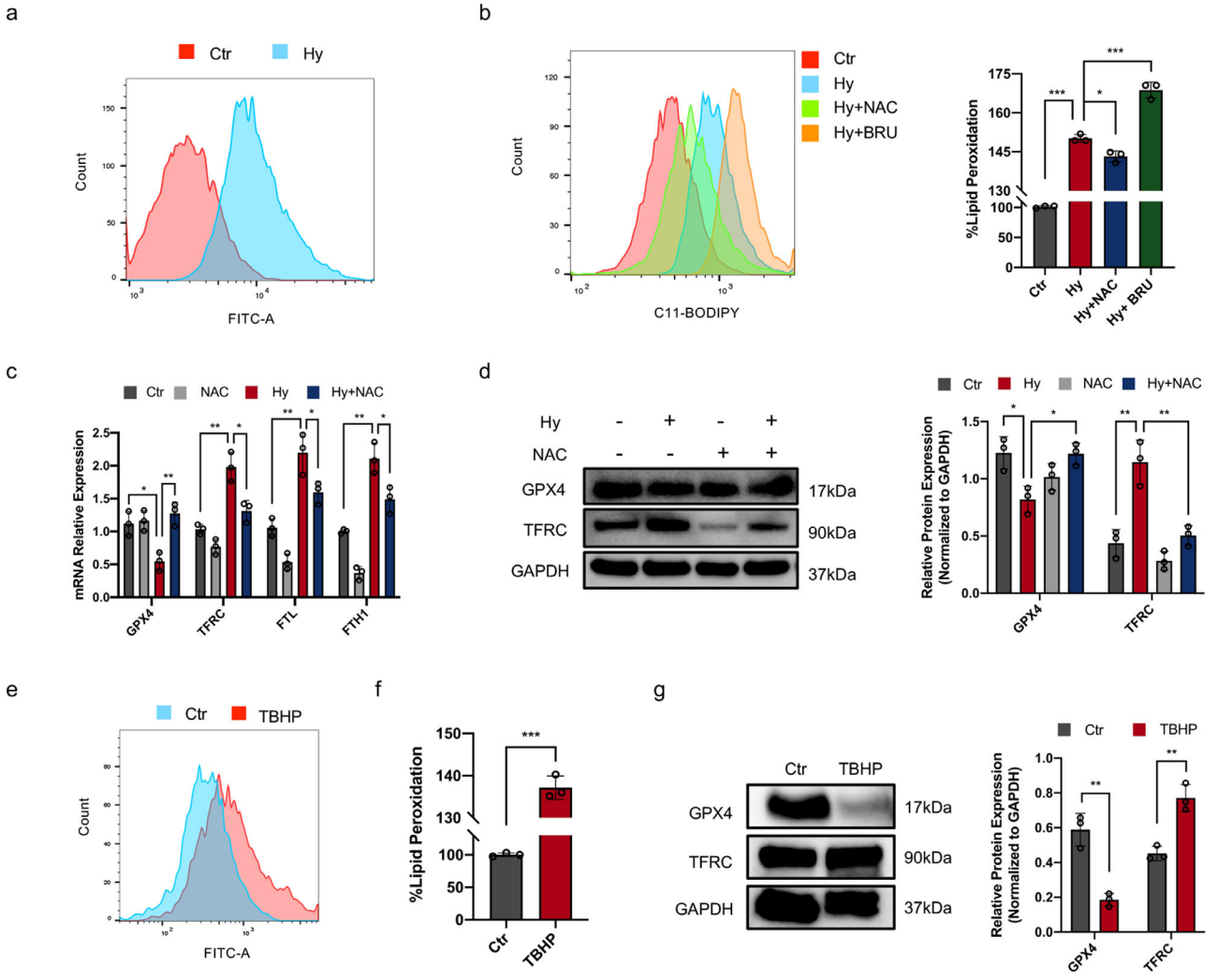

Figure 4. Oxidative stress induces ferroptosis in dry eye. (**a**) ROS levels in HCECs with or without exposure to hyperosmolar stress (500 mOsM, 24 hours) were measured with the H2DCFDA probe using flow cytometry. (**b**) HCECs were cultured in normal or hyperosmotic medium with or without NAC (1 mM) and BRU (50 nM) for 24 hours. Then, lipid peroxidation was evaluated with the BODIPY 581/591-C11 probe using flow cytometry. $N = 3$ per group. (**c**) The mRNA expression levels of GPX4, TFRC, FTL, and FTH1 were evaluated by qRT-PCR. $N = 3$ per group. (**d**) Representative immunoblots for GPX4 and TFRC. Glyceraldehyde-3-phosphate dehydrogenase (GAPDH) was used as the loading control. Relative protein expression levels were calculated with ImageJ and normalized to GAPDH. $N = 3$ per group. (**e**) ROS levels in HCECs treated or not treated with *tert*-butyl hydroperoxide (TBHP, 400 µM, 6 hours) were measured with the H2DCFDA probe using flow cytometry. (**f**) Lipid peroxidation was evaluated with the BODIPY 581/591-C11 probe using flow cytometry. $N = 3$ per group. (**g**) Representative immunoblots for GPX4 and TFRC. GAPDH was used as the loading control. Relative protein expression levels were calculated with ImageJ and normalized to GAPDH. $N = 3$ per group. $^{*}P < 0.05$, $^{**}P < 0.01$, $^{***}P < 0.001$.

stress. After *tert*-butyl hydroperoxide treatment, the levels of total ROS and lipid peroxidation were consistently shown to be increased (Figs. 4e, f), and the expression of GPX4 was significantly downregulated, accompanied by marked upregulation of TFRC (Fig. 4g). These data proved that oxidative stress participated in inducing ferroptosis in HCECs in DED.

AKR1C1 Activation Protects HCECs From Ferroptosis-Mediated Damage In Vitro

We took advantage of the results from previous RNA sequencing, which indicated that the expression of AKR1Cs (AKR1C1–3) obviously increased in genes related to the response to oxidative stress (Fig. 5a, Supplementary Table S6). AKR1Cs are a family of oxidoreductases with the ability to detoxify cytotoxic aldehydes, which are produced during lipid peroxidation.[29] To determine the function of AKR1Cs in ferroptosis in dry eye, HCECs were exposed to hyperosmolarity in the presence or absence of medroxyprogesterone (MPA), a paninhibitor of AKR1C1–3.[30] The data shown in Fig. 5c suggest that the combined hypertonic medium and MPA treatment notably decreased cell viability. To determine which AKR1C family member plays the most pivotal protective role, we transfected HCECs with si-AKR1C1, si-AKR1C2, and si-AKR1C3 separately to inhibit the expression of the three enzymes. The silencing efficiency was confirmed by qRT-PCR (Supplementary Fig. S4b–d). Our results demonstrated that the viability of hypertonic HCECs with AKR1C1 knockdown exhibited the most significant decrease (Fig. 5d). Moreover, the fold changes in

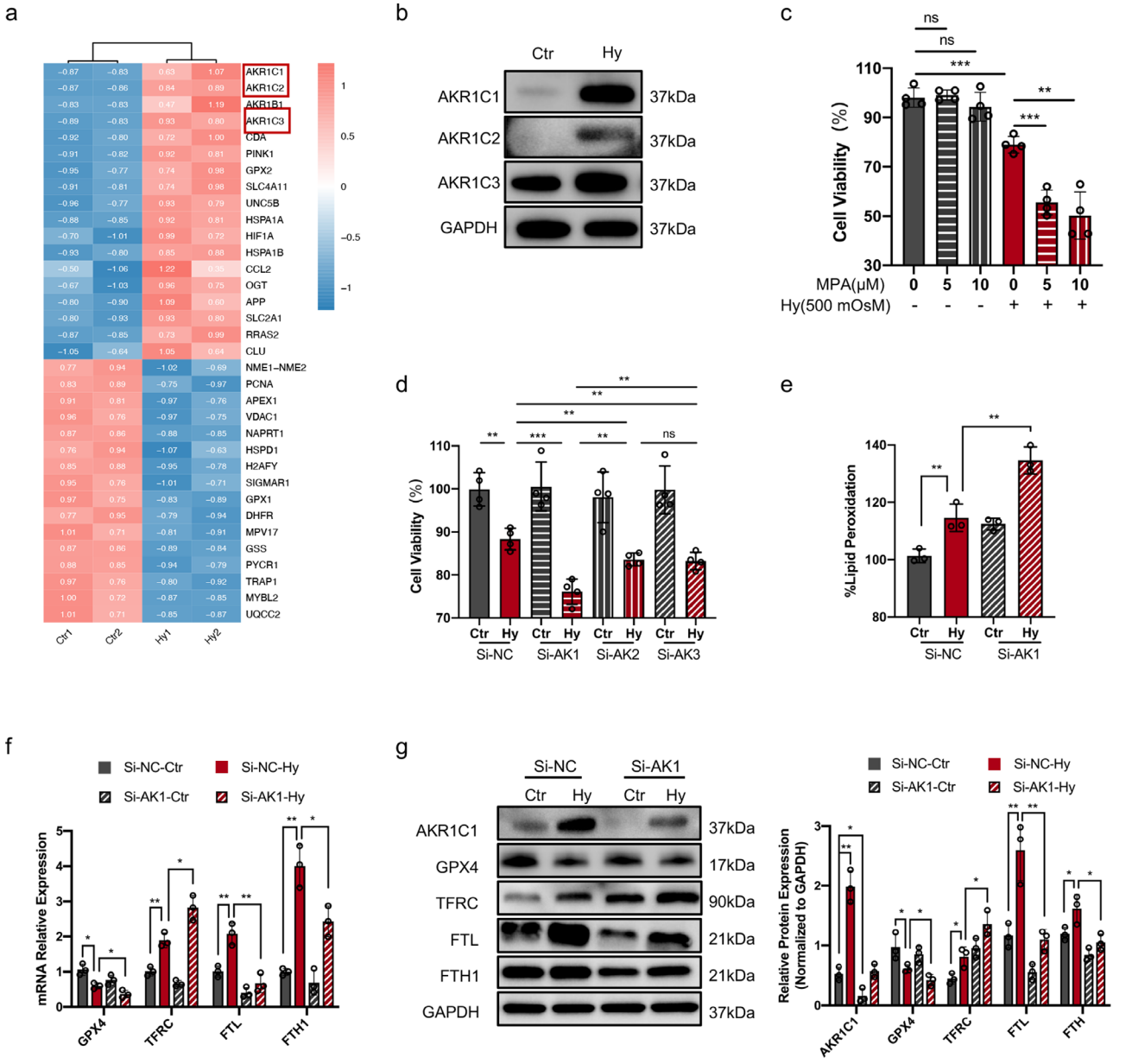

Figure 5. Inhibition of AKR1C1 promotes ferroptosis in HCECs exposed to hyperosmolarity. (**a**) Heatmap showing the transcriptional changes in genes related to the response to oxidative stress in HCECs cultured in hyperosmotic medium (Hy, 500 mOsM) relative to those cultured in normal medium (Ctr) for 24 hours. The normalized data are shown in the modules. (**b**) Representative immunoblots for AKR1C1, AKR1C2, and AKR1C3. (**c**) HCECs were cultured in normal or hyperosmotic medium for 24 hours and were then treated with MPA (0, 5, or 10 μM for 24 hours). Then, cell viability was measured by a CCK-8 assay. $N = 4$ per group. (**d**) HCECs were exposed to hyperosmolarity for 24 hours after transfection with scramble siRNA (si-NC), si-AKR1C1, si-AKR1C2, and si-AKR1C3 for 24 hours. Then, cell viability was measured by a CCK-8 assay. $N = 4$ per group. (**e**) Lipid peroxidation was evaluated with the BODIPY 581/591-C11 probe using flow cytometry. $N = 3$ per group. (**f**) The mRNA expression levels of GPX4, TFRC, FTL, and FTH1 were evaluated by qRT-PCR. $N = 3$ per group. (**g**) Representative immunoblots for AKR1C1, GPX4, TFRC, FTL, and FTH1. Glyceraldehyde-3-phosphate dehydrogenase (GAPDH) was used as the loading control. Relative protein expression levels were calculated with ImageJ and normalized to GAPDH. $N = 3$ per group. ns, $P > 0.05$, $^{*}P < 0.05$, $^{**}P < 0.01$, $^{***}P < 0.001$.

AKR1C1 mRNA and protein expression levels were the greatest among the three groups (Fig. 5b and Supplementary Fig. S4a). Therefore, we detected the lipid peroxidation level and the expression of key ferroptosis-related markers (GPX4, TFRC, FTL, and FTH1) in HCECs with AKR1C1 knockdown under hyperosmolarity. As shown in Figs. 5e–g, lipid peroxidation level increased and the expression of GPX4, FTL, and FTH1 decreased, accompanied by the increased expression of TFRC, which indicated that the ferroptosis was promoted when AKR1C1 was knocked down. Next, we overexpressed AKR1C1 in HCECs. As previously described, the overexpression efficiency was proven by qRT-PCR 36 hours after infection (Supplementary Fig. S4e). As expected, cell viability in the AKR1C1 group (HCECs infected by the AKR1C1-specific overexpression vector) increased significantly, accompanied by a decreased lipid peroxidation level

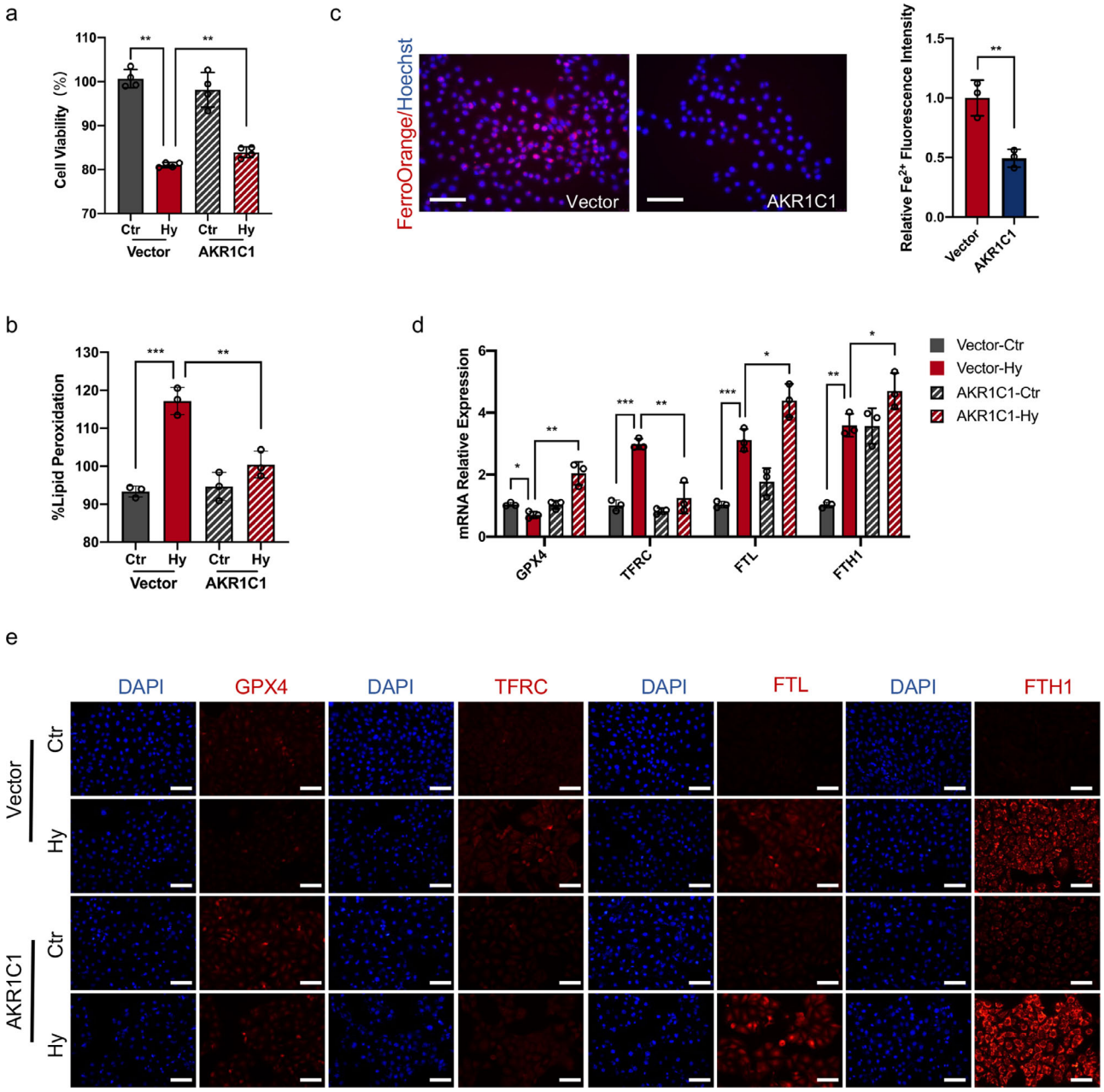

Figure 6. Overexpression of AKR1C1 suppresses ferroptosis in vitro. (**a**) HCECs were exposed to hyperosmolarity for 24 hours after transduction with the AKR1C1-specific overexpression vector or empty vector for 36 hours. Then, cell viability was measured by a CCK-8 assay. $N = 4$ per group. (**b**) Lipid peroxidation was evaluated with the BODIPY 581/591-C11 probe using flow cytometry. $N = 3$ per group. (**c**) Intracellular Fe^{2+} in vector- or AKR1C1-overexpressing HCECs under hyperosmolar stress was detected with the FerroOrange probe under an inverted fluorescence microscope (*blue*, Hoechst-stained nuclei; *red*, FerroOrange-stained Fe^{2+}). Scale bar, 100 µm. Fe^{2+} fluorescence intensity was quantified by ImageJ. (**d**) The mRNA expression levels of GPX4, TFRC, FTL, and FTH1 were measured by qRT-PCR. $N = 3$ per group. (**e**) Representative fluorescence images showing the expression of GPX4, TFRC, FTL, and FTH1. Scale bar, 100 µm. $^{*}P < 0.05$, $^{**}P < 0.01$, $^{***}P < 0.001$.

and iron content, compared with that in the vector group (HCECs infected by the empty vector) (Figs. 6a–c). The mRNA and protein expression levels of key ferroptosis-related markers (GPX4, TFRC, FTL, and FTH1) indicated that ferroptosis was suppressed by the overexpression of AKR1C1 (Figs. 6d, e). Taken together, our results indicated that the upregulation of AKR1C1 can protect HCECs against ferroptosis and partially offset the cell damage induced by hyperosmolarity.

NRF2 Upregulates AKR1C1 in HCECs Under Hypertonic Stress

Our previous results revealed that AKR1C1 is a key enzyme protecting against HCEC ferroptosis in dry eye; thus, we sought to investigate the molecular mechanism regulating AKR1C1 expression. The antioxidant system is simultaneously activated when ROS accumulate excessively in cells, and the canonical transcription factor NRF2 is an important

Investigative Ophthalmology & Visual Science

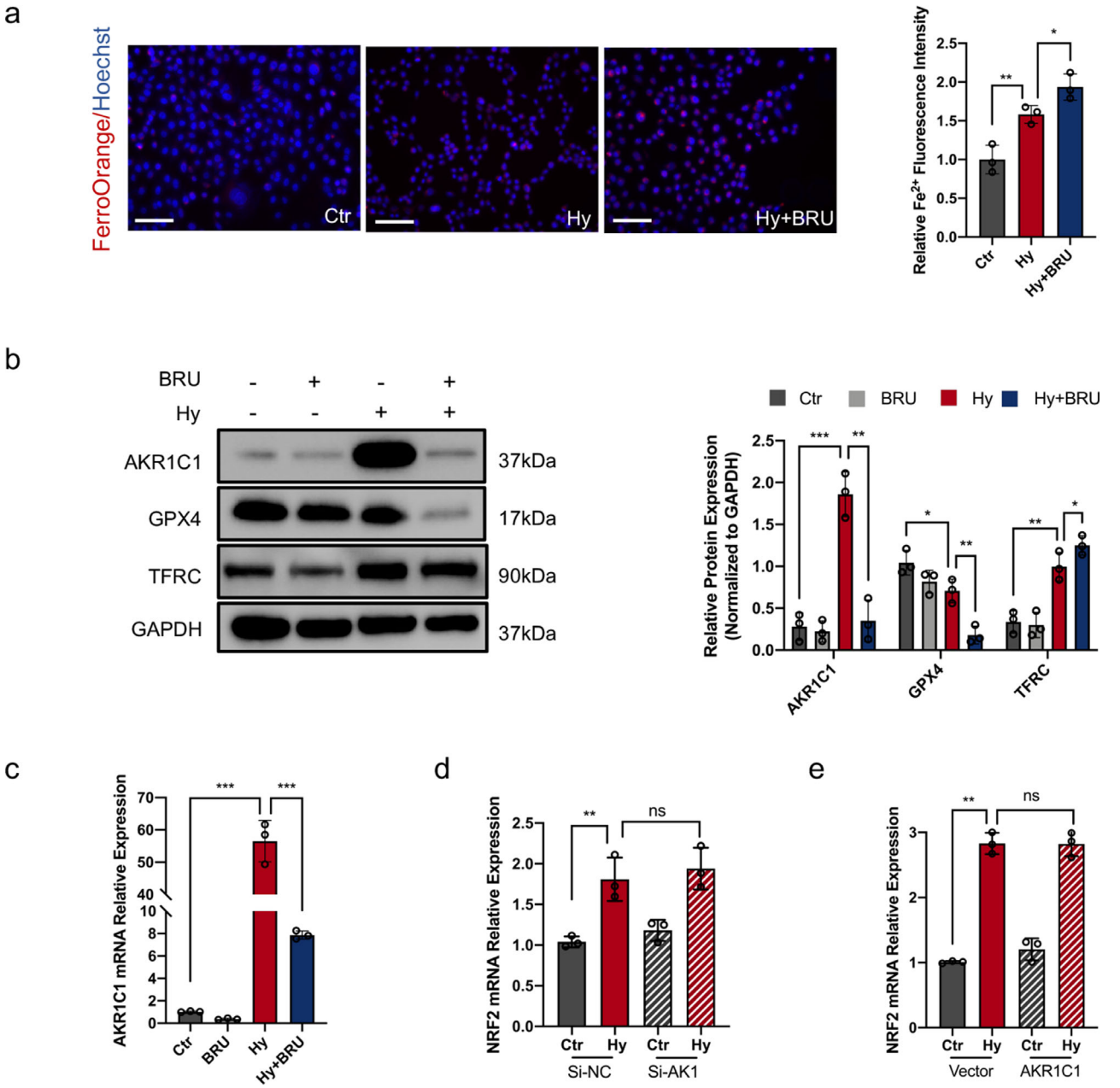

Figure 7. NRF2 upregulates AKR1C1 to protect against ferroptosis in HCECs under hyperosmolar stress. (**a**) HCECs were cultured in normal or hyperosmotic medium with or without BRU (50 nM) for 24 hours. Then, intracellular Fe^{2+} was detected with the FerroOrange probe under an inverted fluorescence microscope (blue, Hoechst-stained nuclei; red, FerroOrange-stained Fe^{2+}). Scale bar, 100 µm. Fe^{2+} fluorescence intensity was quantified by ImageJ. (**b**) Representative immunoblots for AKR1C1, GPX4, and TFRC. Glyceraldehyde-3-phosphate dehydrogenase (GAPDH) was used as the loading control. Relative protein expression levels were calculated with ImageJ and normalized to GAPDH. $N = 3$ per group. (**c**) The expression level of AKR1C1 was measured by qRT-PCR. $N = 3$ per group. (**d**) The expression level of NRF2 was measured by qRT-PCR in scramble siRNA (si-NC) and si-AK1 HCECs with or without hyperosmolarity exposure. $N = 3$ per group. (**e**) The expression level of NRF2 was measured by qRT-PCR in vector- and AKR1C1-transfected HCECs with or without hyperosmolarity exposure. $N = 3$ per group. ns, $P > 0.05$, $^{*}P < 0.05$, $^{**}P < 0.01$, $^{***}P < 0.001$.

transcription factor regulating the antioxidant pathway.[31] Thus, our investigation focused on NRF2. First, we observed that the expression levels of NRF2 in HCECs under hyperosmolar stress were significantly increased (Supplementary Fig. S5a, b). Furthermore, we confirmed that HCECs underwent more ferroptosis when NRF2 was inhibited by brusatol (BRU), which is reported to be a specific NRF2 inhibitor, as indicated by a marked increase in lipid peroxidation and cellular iron content, a downregulation of GPX4 and the upregulation of TFRC (Fig. 4b, and Figs. 7a, b). Next, we evaluated the regulatory relationship between NRF2 and AKR1C1. Interestingly, the data clearly suggested that the inhibition of NRF2 by BRU resulted in a consistent decrease in hyperosmolarity-mediated AKR1C1 upregulation (Figs. 7b, c). Conversely, the mRNA expression levels of NRF2 were not significantly influenced in hypertonic HCECs

with knockdown or overexpression of AKR1C1 (Figs. 7d, e). Heme oxygenase-1 (HMOX-1) was acknowledged as the most correlated gene in response to NRF2 activation in the antioxidative pathway in DED. However, the knockdown of HMOX-1 decreased cell viability, but had no effect on the lipid peroxidation level in HCECs exposed to hyperosmolarity (Supplementary Fig. S5c, d). Therefore, these results suggested that NRF2 is activated to decrease the level of lipid peroxidation and inhibit ferroptosis in HCECs under the hypertonic state by upregulating AKR1C1 independent of HMOX-1.

Inhibition of AKR1C1 Promotes Dry Eye In Vivo

The findings from cellular studies prompted us to further analyze the function of AKR1C1 in ferroptosis-associated

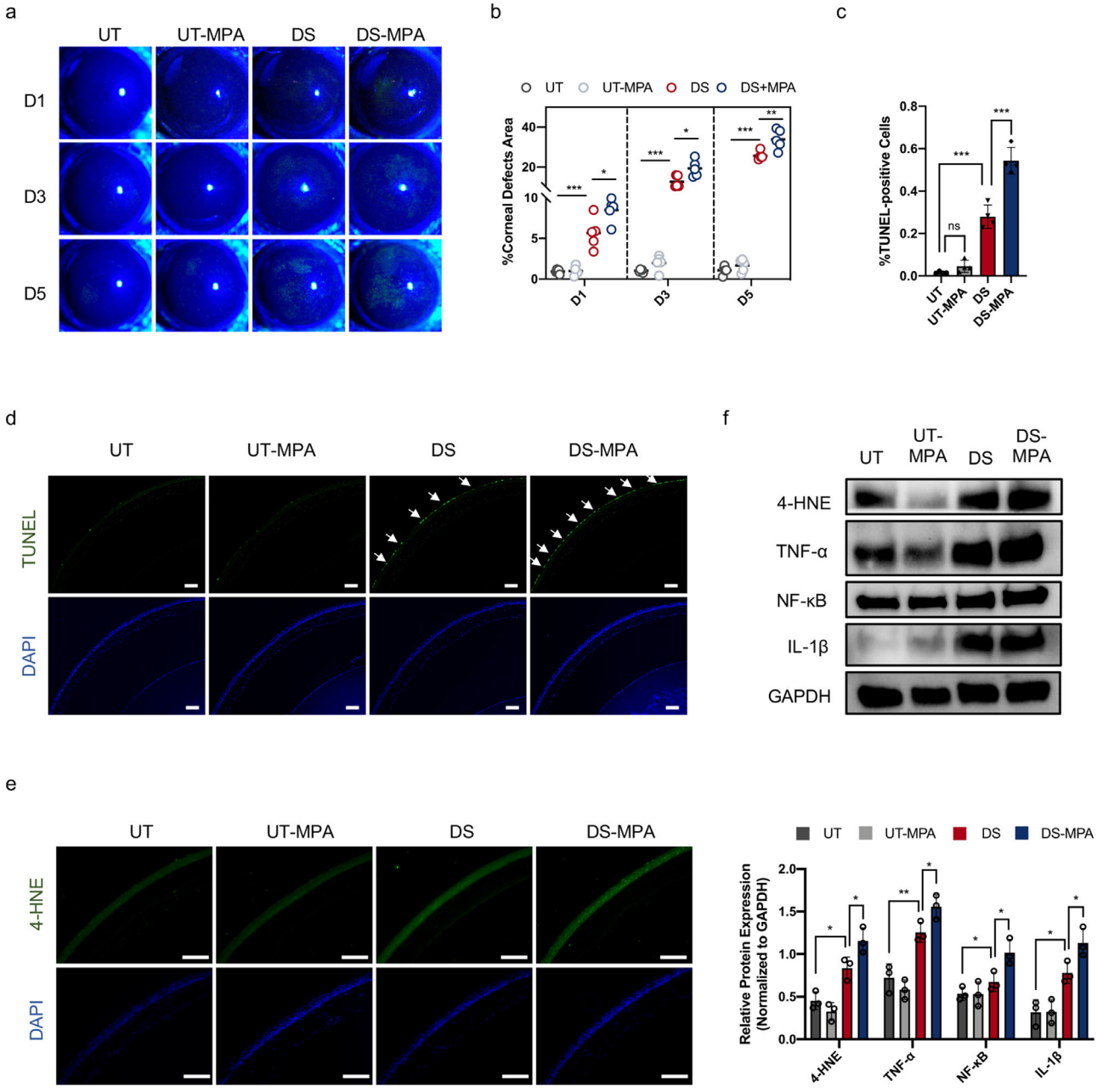

Figure 8. Inhibition of AKR1C1 promotes dry eye in vivo. (**a**) Photographs of corneal fluorescein staining after treatment for 1, 3, and 5 days. (**b**) The corneal defect area (percentage) was calculated with ImageJ. $N = 5$ per group. (**c**) The percentage of TUNEL-positive cells was determined with ImageJ. $N = 4$ per group. (**d**) Representative fluorescence images from the TUNEL assay of corneal epithelium from the untreated (UT) group, UT group with MPA treatment, DS group, and DS group with MPA treatment on day 5 (*blue*, DAPI-stained nuclei; *green*, TUNEL-positive dead cells). *White arrows* indicate TUNEL-positive cells. Scale bar, 100 µm. (**e**) Representative fluorescence images showing the expression of 4-HNE in the corneal epithelium from the UT, UT-MPA, DS and DS-MPA groups on day 5. Scale bar, 100 µm. (**f**) Representative immunoblots for 4-HNE, TNF-α, NF-κB, and IL-1β in the UT, UT-MPA, DS, and DS-MPA groups on day 5. Glyceraldehyde-3-phosphate dehydrogenase (GAPDH) was used as the loading control. Relative protein expression levels were calculated with ImageJ and normalized to GAPDH. $N = 3$ per group. $^{*}P < 0.05$, $^{**}P < 0.01$, $^{***}P < 0.001$.

Investigative Ophthalmology & Visual Science

dry eye in vivo. Because few specific inhibitors targeting AKR1C1 have been identified, MPA was used to inhibit AKR1C1. To examine the possible effect of AKR1C1 on dry eye in vivo, we treated wild-type mice and DED model mice with vehicle (10% DMSO, 400 µL, daily, intraperitoneally) and MPA (1 mg/mL, 400 µL, in 10% DMSO, daily, intraperitoneally). As shown in Figs. 8a–d, DED mice treated with MPA exhibited more severe corneal epithelial defects and incurred more corneal epithelial cell death. The expression of 4-HNE in the DS-MPA group was increased, indicating higher levels of lipid peroxidation than those in the DS group (Figs. 8e, f). Moreover, the data presented in Fig. 8f and Supplementary Fig. S6 indicated that the expression levels of TNF-α, NF-κB, and IL-1β were increased in DED mice after inhibition of AKR1C1 by MPA. Taken together, these in vivo results suggested that activation of AKR1C1 protected corneal epithelial cells from lipid peroxidative damage and relieved the inflammatory response in DED.

Discussion

A vicious cycle of ocular surface inflammation and corneal epithelial defects has been shown to promote the development of DED.[6,32] Previous research suggested that the modes of corneal epithelial cell death in DED mainly include necrosis and apoptosis. Moreover, pyroptosis was recently confirmed to be involved in the pathogenesis of dry eye.[5] In the present study, our RNA-seq analysis of corneal epithelial cells showed that the mRNA expression of ferroptotic factors has increased and that of antiferroptotic factors has decreased in DED. Furthermore, the increase in the intracellular iron content combined with the accumulation of lipid peroxides induced by excessive oxidative stress indicated that ferroptosis might occur in dry eye. During this process, we also found that AKR1C1 was markedly upregulated via NRF2, which played a vital role in preventing ferroptosis.

Ferroptosis has been reported to be closely correlated with numerous human diseases, such as acute kidney injury, neurological disorders, and various tumors; however, there is a lack of research on the change and function of ferroptosis in dry eye.[16,33,34] Here, we provide the first evidence of the occurrence of ferroptosis in dry eye. Cysteine metabolism, iron metabolism, and lipid metabolism are acknowledged to be indispensable for ferroptosis induction.[19] Indeed, we found that ferroptosis in DED was accompanied by the inhibition of GPX4, the accumulation of intracellular iron, and an increased expression of ACSL4. However, our results in vivo and in vitro did not point to the same, exact mechanism of ferroptosis. Our data revealed that a decrease in GPX4 expression and accumulation of intracellular iron were the main contributors to ferroptosis induction in vitro, whereas lipid metabolism regulated by ACSL4 may be the core mechanism of ferroptosis in vivo. Notably, the protein expression of ACSL4 differed between HCECs exposed to hyperosmolarity and DED mice. Some recent studies have suggested that the expression of ACSL4 seems to be a predictive marker for ferroptosis sensitivity.[35,36] In our research, we indeed found that the viability of HCECs has decreased under relatively high concentrations of the ferroptosis inducers erastin and RSL3 in vitro. The marked upregulation of ACSL4 in DED mice may indicate that corneal epithelial cells under DS were more sensitive to ferroptosis, which calls for a need for this phenomenon to be explored in the future. Admittedly, the precise correlation of ferroptosis in vivo and in vitro still needs to be studied in greater depth. In general, our study enhanced the understanding of the pathogenic mechanism related to cell death in corneal epithelial cells in DED.

Iron homeostasis is essential for maintaining the normal physiological activities of the cell.[37] An aberrant accumulation of iron damages organelles and cell membranes by producing massive amounts of lipid ROS and thereby inducing ferroptosis.[13,14] Intracellular iron levels are controlled by regulatory factors, including TFRC, FTL, and FTH1. Increased expression of TFRC, the central regulator, leads to an increase in the flux of iron into the cell. The iron storage protein complex composed of FTL and FTH1 can bind to free iron to decrease cell damage.[38,39] Most of the current literature suggests that FTL and FTH1 are downregulated in the process of ferroptosis.[14,40] However, we observed that TFRC, FTL and FTH1 were simultaneously upregulated in HCECs exposed to hyperosmolarity. We speculated that increased expression of TFRC led to an increase in iron transported into the cell, which in turn promoted the synthesis of iron-binding proteins. Consistent with this hypothesis, the increased content of iron shown by iron staining demonstrated that the upregulation of iron storage proteins failed to eliminate excess Fe^{2+}. Hence, our results suggested that the increases in FTL and FTH1 expression were mediated by excessive intracellular Fe^{2+} content during ferroptosis, indicating that a comprehensive analysis of the final content of iron as well as ferroptosis-related proteins was necessary.

The AKR1C family has been reported to be involved in various human cancers.[21,41] The overexpression of AKR1Cs has been identified as a marker of the growth and progression of tumors and found to promote metastasis and drug resistance in cancer.[25,26] Interestingly, we found that AKR1Cs were prominently activated in HCECs under hyperosmolar stress. Furthermore, cell viability was significantly decreased after the inhibition of AKR1Cs, especially AKR1C1. In vivo, ocular surface defects and the inflammatory response in DED mice were promoted by MPA, an inhibitor of AKR1Cs. In contrast, the overexpression of AKR1C1 abated the cell damage caused by ferroptosis. Therefore, our results revealed that AKR1C1 was strikingly activated by hyperosmolarity to encourage HCECs to guard against lipid peroxidation-related ferroptosis. Moreover, the knockdown of AKR1C1 had a greater impact on the expression of TFRC and FTL than GPX4, indicating that AKR1C1 suppressed ferroptosis primarily by stabilizing the balance of iron metabolism. However, we observed that the protective effect of AKR1C1 was limited, because HCECs still underwent partial ferroptosis under hypertonic stimulation, even when AKR1C1 was artificially overexpressed. Nevertheless, our research proposes a novel theory that the upregulation of AKR1C1 protects corneal epithelial cells against ferroptosis in DED, providing a potential gene target for DED therapy.

Several studies have shown that NRF2 facilitates cellular redox homeostasis by regulating the expression of many antioxidative enzymes, including thioredoxin reductase 1, NAD(P)H-quinone oxidoreductase 1, and HMOX1.[42,43] Among pathways related to these enzymes, the NRF2/HMOX-1 pathway has been acknowledged as an important antioxidative and antiapoptotic mechanism in DED,[44,45] an assertion that was also confirmed in our previous research efforts. In our current study, we discovered that the regulation of HMOX-1 affected the cell viability percentage, but had no significant influence on the lipid peroxidation level in dry eye. However, the specific NRF2 inhibitor BRU significantly exacerbated ferroptosis by suppressing AKR1C1 expression. Thus, these results strongly

Investigative Ophthalmology & Visual Science

indicated that NRF2 probably inhibits ferroptosis by activating AKR1C1 independent of the classic factor HMOX-1. These data provide a novel option for the NRF2/AKR1C1 pathway to protect against ferroptosis-induced damage in HCECs and enrich and expand the understanding of the mechanistic network of NRF2 in the pathogenesis of DED.

Recently, several studies have suggested that ferroptosis is a form of necrotic death that induces cells to release damage-associated molecular patterns, which amplify immune cell infiltration and the inflammatory response.[46,47] In contrast, some research has reported that ferroptosis may be a therapeutic physiological process protecting against both inflammatory and neoplastic processes.[48,49] These conflicting results emphasize the importance of further illustrating the relationship between ferroptosis and inflammation in DED. Our results indicated that the inhibition of ferroptosis by Fer-1 alleviated corneal defects and effectively decreased the expression of NF-κB, TNF-α, and IL-1β in DED model mice. Moreover, the ocular surface inflammation was significantly increased when ferroptosis was promoted by the inhibition of AKR1Cs. Therefore, we revealed that ferroptosis might participate in promoting the inflammatory response in dry eye, however, the specific molecular pathway linking ferroptosis and ocular surface inflammation needs further investigation.

Conclusions

Our results provide evidence that oxidative stress-induced ferroptosis participates in the death of corneal epithelial cells in DED. The upregulation of AKR1C1 mediated by NRF2 plays a significant role in protecting against cell damage caused by lipid peroxidation. The inhibition of ferroptosis can rescue corneal defects and alleviate the inflammatory response. Our study thus provides a potential therapeutic strategy for DED based on antiferroptotic drugs combined with AKR1C1 activators.

Acknowledgments

The authors gratefully thank Xihong Lan (State Key Laboratory of Ophthalmology, Zhongshan Ophthalmic Center, Sun Yat-sen University) for technical support with the flow cytometry work and Jing Zhang (Wilmer Eye Institute, Johns Hopkins University School of Medicine) for help with improving the language of the article.

Supported by the National Natural Science Foundation of China to JY (No. 82171015), Projects of International Cooperation and Exchanges NSFC to HO (No. 32061160364), and the National Natural Science Foundation of China to BW (No. 82101083). The funding organization played no role in the design or execution of this research.

Author contributions: XZ and HZ performed the experiments, analyzed the data, and wrote the manuscript; BW, XY, and DH performed the experiments and interpreted the results. LW and HO provided technical and material support. JY designed the study and reviewed and revised the paper. All authors read and approved the final paper.

Ethics: All animal experiments complied with the Association for Research in Vision and Ophthalmology Statement for the Use of Animals in Ophthalmic and Vision Research and were approved by the Institutional Review Board of Zhongshan Ophthalmic Center (Guangzhou, China; approval ID: 2020-138).

Data Availability Statement: The datasets used and analyzed during the current study are available from the corresponding author on reasonable request.

Disclosure: **X. Zuo**, None; **H. Zeng**, None; **B. Wang**, None; **X. Yang**, None; **D. He**, None; **L. Wang**, None; **H. Ouyang**, None; **J. Yuan**, None

References

1. Stapleton F, Alves M, Bunya VY, et al. TFOS DEWS II epidemiology report. *Ocul Surf*. 2017;15:334–365.
2. Kojima T, Dogru M, Kawashima M, Nakamura S, Tsubota K. Advances in the diagnosis and treatment of dry eye. *Prog Retin Eye Res*. 2020:100842.
3. Shimazaki J. Definition and diagnostic criteria of dry eye disease: historical overview and future directions. *Invest Ophthalmol Vis Sci*. 2018;59:DES7–DES12.
4. Pflugfelder SC, de Paiva CS. The pathophysiology of dry eye disease: what we know and future directions for research. *Ophthalmology*. 2017;124:S4–S13.
5. Chen H, Gan X, Li Y, et al. NLRP12- and NLRC4-mediated corneal epithelial pyroptosis is driven by GSDMD cleavage accompanied by IL-33 processing in dry eye. *Ocul Surf*. 2020;18:783–794.
6. Seen S, Tong L. Dry eye disease and oxidative stress. *Acta Ophthalmol*. 2018;96:e412–e420.
7. Sacca SC, Cutolo CA, Ferrari D, Corazza P, Traverso CE. The eye, oxidative damage and polyunsaturated fatty acids. *Nutrients*. 2018;10:668.
8. Hybertson BM, Gao B, Bose SK, McCord JM. Oxidative stress in health and disease: the therapeutic potential of Nrf2 activation. *Mol Aspects Med*. 2011;32:234–246.
9. Brieger K, Schiavone S, Miller FJ, Krause KH. Reactive oxygen species: from health to disease. *Swiss Med Wkly*. 2012;142:w13659.
10. Zhou J, Ge L, Jia C, et al. ROS-mediated different homeostasis of murine corneal epithelial progenitor cell line under oxidative stress. *Sci Rep*. 2016;6:36481.
11. Wang B, Peng L, Ouyang H, et al. Induction of DDIT4 impairs autophagy through oxidative stress in dry eye. *Invest Ophthalmol Vis Sci*. 2019;60:2836–2847.
12. Wang B, Zuo X, Peng L, et al. Melatonin ameliorates oxidative stress-mediated injuries through induction of HO-1 and restores autophagic flux in dry eye. *Exp Eye Res*. 2021;205:108491.
13. Dixon SJ, Lemberg KM, Lamprecht MR, et al. Ferroptosis: an iron-dependent form of nonapoptotic cell death. *Cell*. 2012;149:1060–1072.
14. Li J, Cao F, Yin HL, et al. Ferroptosis: past, present and future. *Cell Death Dis*. 2020;11:88.
15. Lee H, Zandkarimi F, Zhang Y, et al. Energy-stress-mediated AMPK activation inhibits ferroptosis. *Nat Cell Biol*. 2020;22:225–234.
16. Xie Y, Hou W, Song X, et al. Ferroptosis: process and function. *Cell Death Differ*. 2016;23:369–379.
17. Angeli JPF, Schneider M, Proneth B, et al. Inactivation of the ferroptosis regulator Gpx4 triggers acute renal failure in mice. *Nat Cell Biol*. 2014;16:1180–1191.
18. Gao M, Monian P, Quadri N, Ramasamy R, Jiang X. Glutaminolysis and transferrin regulate ferroptosis. *Mol Cell*. 2015;59:298–308.
19. Chen X, Li J, Kang R, Klionsky DJ, Tang D. Ferroptosis: machinery and regulation. *Autophagy*. 2020;17:2054–2081.
20. Yuan H, Li X, Zhang X, Kang R, Tang D. Identification of ACSL4 as a biomarker and contributor of ferroptosis. *Biochem Biophys Res Commun*. 2016;478:1338–1343.

21. Penning TM. The aldo-keto reductases (AKRs): overview. *Chem Biol Interact*. 2015;234:236–246.
22. Gagliardi M, Cotella D, Santoro C, et al. Aldo-keto reductases protect metastatic melanoma from ER stress-independent ferroptosis. *Cell Death Dis*. 2019;10:902.
23. Penning TM. Aldo-keto reductase regulation by the Nrf2 system: implications for stress response, chemotherapy drug resistance, and carcinogenesis. *Chem Res Toxicol*. 2017;30:162–176.
24. Lyon RC, Li D, McGarvie G, Ellis EM. Aldo-keto reductases mediate constitutive and inducible protection against aldehyde toxicity in human neuroblastoma SH-SY5Y cells. *Neurochem Int*. 2013;62:113–121.
25. Zeng CM, Chang LL, Ying MD, et al. Aldo-keto reductase AKR1C1-AKR1C4: functions, regulation, and intervention for anti-cancer therapy. *Front Pharmacol*. 2017;8:119.
26. Penning TM, Jonnalagadda S, Trippier PC, Rizner TL. Aldo-keto reductases and cancer drug resistance. *Pharmacol Rev*. 2021;73:1150–1171.
27. Miotto G, Rossetto M, Di Paolo ML, et al. Insight into the mechanism of ferroptosis inhibition by ferrostatin-1. *Redox Biol*. 2020;28:101328.
28. Zhong H, Yin H. Role of lipid peroxidation derived 4-hydroxynonenal (4-HNE) in cancer: focusing on mitochondria. *Redox Biol*. 2015;4:193–199.
29. Penning TM, Wangtrakuldee P, Auchus RJ. Structural and functional biology of aldo-keto reductase steroid-transforming enzymes. *Endocr Rev*. 2019;40:447–475.
30. Barski OA, Tipparaju SM, Bhatnagar A. The aldo-keto reductase superfamily and its role in drug metabolism and detoxification. *Drug Metab Rev*. 2008;40:553–624.
31. Loboda A, Damulewicz M, Pyza E, Jozkowicz A, Dulak J. Role of Nrf2/HO-1 system in development, oxidative stress response and diseases: an evolutionarily conserved mechanism. *Cell Mol Life Sci*. 2016;73:3221–3247.
32. Clayton JA. Dry eye. *N Engl J Med*. 2018;378:2212–2223.
33. Mou Y, Wang J, Wu J, et al. Ferroptosis, a new form of cell death: opportunities and challenges in cancer. *J Hematol Oncol*. 2019;12:34.
34. Weiland A, Wang Y, Wu W, et al. Ferroptosis and its role in diverse brain diseases. *Mol Neurobiol*. 2019;56:4880–4893.
35. Doll S, Proneth B, Tyurina YY, et al. ACSL4 dictates ferroptosis sensitivity by shaping cellular lipid composition. *Nat Chem Biol*. 2017;13:91–98.
36. Li Y, Feng D, Wang Z, et al. Ischemia-induced ACSL4 activation contributes to ferroptosis-mediated tissue injury in intestinal ischemia/reperfusion. *Cell Death Differ*. 2019;26:2284–2299.
37. Recalcati S, Gammella E, Cairo G. Dysregulation of iron metabolism in cancer stem cells. *Free Radic Biol Med*. 2019;133:216–220.
38. Ye J, Wang Z, Chen X, et al. YTHDF1-enhanced iron metabolism depends on TFRC m(6)A methylation. *Theranostics*. 2020;10:12072–12089.
39. Arosio P, Elia L, Poli M. Ferritin, cellular iron storage and regulation. *IUBMB Life*. 2017;69:414–422.
40. Li Z, Jiang L, Chew SH, Hirayama T, Sekido Y, Toyokuni S. Carbonic anhydrase 9 confers resistance to ferroptosis/apoptosis in malignant mesothelioma under hypoxia. *Redox Biol*. 2019;26:101297.
41. Mindnich RD, Penning TM. Aldo-keto reductase (AKR) superfamily: genomics and annotation. *Hum Genomics*. 2009;3:362–370.
42. Ma Q. Role of nrf2 in oxidative stress and toxicity. *Annu Rev Pharmacol Toxicol*. 2013;53:401–426.
43. Sajadimajd S, Khazaei M. Oxidative stress and cancer: the role of Nrf2. *Curr Cancer Drug Targets*. 2018;18:538–557.
44. Dai Y, Zhang J, Xiang J, Li Y, Wu D, Xu J. Calcitriol inhibits ROS-NLRP3-IL-1beta signaling axis via activation of Nrf2-antioxidant signaling in hyperosmotic stress stimulated human corneal epithelial cells. *Redox Biol*. 2019;21:101093.
45. Zhang Y, An Y, He X, Zhang D, He W. Esculetin protects human corneal epithelial cells from oxidative stress through Nrf-2 signaling pathway. *Exp Eye Res*. 2021;202:108360.
46. Sun Y, Chen P, Zhai B, et al. The emerging role of ferroptosis in inflammation. *Biomed Pharmacother*. 2020;127:110108.
47. Li W, Feng G, Gauthier JM, et al. Ferroptotic cell death and TLR4/Trif signaling initiate neutrophil recruitment after heart transplantation. *J Clin Invest*. 2019;129:2293–2304.
48. Ebel P, Imgrund S, Vom Dorp K, et al. Ceramide synthase 4 deficiency in mice causes lipid alterations in sebum and results in alopecia. *Biochem J*. 2014;461:147–158.
49. Arbiser JL, Bonner MY, Ward N, Elsey J, Rao S. Selenium unmasks protective iron armor: a possible defense against cutaneous inflammation and cancer. *Biochim Biophys Acta Gen Subj*. 2018;1862:2518–2527.

Investigative Ophthalmology & Visual Science